ChemPubSoc Europe

DOI: 10.1002/cphc.201300293

Effects of Oriented Surface Dipole on Photoconversion Efficiency in an Alkane/Lipid-Hybrid-Bilayer-Based Photovoltaic Model System

Lixia Liu,[a] Hong Xie,[a] Heidi E. Bostic,[b] Limei Jin,[c] Michael D. Best,[b] X. Peter Zhang,[c] and Wei Zhan*[a]

When a phospholipid monolayer containing a zinc-coordinated porphyrin species formed atop a self-assembled monolayer of heptadecafluoro-1-decanethiol ($CF_3(CF_2)_7(CH_2)_2SH$) is subjected to photoelectrochemical current generation, a significant modulation effect is observed. Compared with devices that contain similar photoactive lipid monolayers but formed on 1-dodecanethiol SAMs, these fluorinated hybrid bilayers produce a $>60\%$ increase in cathodic currents and a similar decrease in anodic currents. Photovoltages recorded from these hybrid bilayers are found to vary in the same fashion. The modulation of photovoltaic responses in these hybrid-bilayer-based devices is explained by the opposite surface dipoles associated with the thiols employed in this study, which in one case (fluorothiol) increase and in another (alkanethiol) decrease the work function of the underlying gold substrates. A similar trend of photovoltage/photocurrent modulation is also observed if fullerene is used as the photoagent in these devices. Our results reveal the intricacy of orientated surface dipole in influencing the photovoltaic processes, and its subtle interplay with other factors related to the photoagents, such as their location and orientation within the organic matrix.

1. Introduction

Unlike single-crystalline semiconductor solar cells, light excitation in low-dielectric organic solar devices initially generates excitons and polarons, for which separation into free charge carriers critically depends on the interfacial and morphological characteristics of the organic matrices.[1,2] It can be difficult to understand each of these properties at device level as they often appear convoluted and interdependent. To this end, recent research based on theoretical modeling[3,4] has proved to be very fruitful. Experimentally, molecular model architectures, based on single donor/acceptor layers,[5–7] are ideally suited to study various interfacial processes in organic photovoltaics (OPV). We have successfully introduced several solid-supported lipid bilayer structures into the study of photoinduced electron transfer processes at water/lipid/electrode interfaces.[8–11] These systems allow a series of parameters critical to fundamental photovoltaic processes to be accessed, often in well-defined single-component settings. Control of dosing, positioning and directionality of multiple electron donors/acceptors (synthetic or natural) in a single bilayer can be thus achieved. By using porphyrin and fullerene as model photoagents, we report here that polar alkanethiols included in these bilayers can significantly modulate the resulting photovoltaic responses. These results not only allow us to make connections with the practice in organic electronic devices of using polar organic adsorbates to tune the work function of metals and hence the charge injection efficiency, but also highlight the subtle interplay of orientated surface dipole with other factors related to the photoagents, such as their location and orientation, in an alkanethiol/lipid bilayer matrix.

Of particular relevance is the research in organic light-emitting diodes (LEDs) and other related fields that employ polar organic adsorbates to tune the work function of electrode materials and hence the charge injection barriers. The fundamental concept[12] here is the use of an organic layer to modify the potential difference (ζ) of electrons inside and outside a metal, which is related to the metal work function (φ_m) by the equation $\varphi_m = \zeta - E_F$, in which E_F is the Fermi level of the metal. The importance of ζ in affecting the work function of metals was recognized as early as the 1930s, when a monolayer of alkali atoms was found to reduce φ_m of metals by more than half in a study of photoelectric effects.[13,14] These experimental observations made Bardeen realize that work function is essentially a surface property of a metal that is determined largely by its uppermost atomic layers.[15] More recently, Campbell and coworkers[16] demonstrated that thiols, which self-assembled on noble metals could be fruitfully used to tune the work function

[a] L. Liu, Dr. H. Xie, Prof. W. Zhan
Department of Chemistry and Biochemistry
Auburn University
Auburn, AL 36849 (USA)
E-mail: wzz0001@auburn.edu

[b] Dr. H. E. Bostic, Prof. M. D. Best
Department of Chemistry
The University of Tennessee
Knoxville, TN 37996 (USA)

[c] Dr. L. Jin, Prof. X. P. Zhang
Department of Chemistry
The University of South Florida
Tampa, FL 33620 (USA)

Supporting information for this article is available on the WWW under http://dx.doi.org/10.1002/cphc.201300293.

of these metals. Generally, if a monolayer of polar alkanethiols is absorbed on a metal, formation of a dipole layer (sometimes called an electrostatic double layer) at the metal/organic interface occurs, which imposes a localized potential that can electrostatically impede or ease the extraction of electrons from the metal. Systematic tuning of the metal work function can be realized by controlling the structure, size and substituent groups of organic absorbates.[17] The reason that such an interfacial dipole layer can affect the charge injection from/to organic materials layered further atop, which sometimes are macroscopic, is because it is positioned within the charge injection path. Owing to the ease of preparation and well-defined structures of self-assembled thiols on noble metals, this method has since evolved into a versatile and powerful strategy that is widely employed in several fields such as organic LEDs and organic field-effect transistors.[18,19]

More recent work has also shown such a strategy can be successfully employed to control and improve OPV systems. For example, by using a C_{16} self-assembled monolayer (SAM), Mihailetchi et al.[20] were able to lower the silver work function by 0.6 eV, which allowed the researchers to build electron-dominant devices in studying poly(phenylene vinylene)/fullerene-based bulk heterojunction solar cells. In another study, Kim and co-workers[21] showed that enhancement of power conversion efficiency could be achieved in OPV cells fabricated with SAM-covered gold substrates. The effectiveness of using polar SAMs to modify injection barriers for electrogenerated as well as photogenerated charges highlights the general importance of energy alignment in achieving efficient interfacial charge injection.

In this study, we set out to determine quantitatively how SAMs with well-defined dipoles influence the photovoltaic responses of alkanethiol/lipid hybrid bilayer-based model cells. These are arguably one of the simplest models to observe this interesting interfacial phenomenon, with a single dipole layer sandwiched in between an electrode and a photoagent-assembled lipid monolayer. Our results confirm the general trend established by previous studies and in addition, demonstrate the usefulness and controllability of alkanethiol/lipid hybrid structures in probing photovoltaic processes.

2. Results and Discussion

2.1 Construction/Characterization of Hybrid-Bilayer-Based Photocells

Figure 1 shows the structure of alkanethiol/lipid hybrid bilayers and the photoactive agents used in this study. To form such bilayers, a SAM of either dodecanethiol ($C_{12}H_{25}SH$) or heptadecafluoro-1-decanethiol ($C_{10}F_{17}SH$) is first formed on clean gold substrates, which is then covered with a monolayer of phospholipids upon exposure to a liposome solution containing either malonic fullerene or DOPE-conjugated zinc porphyrin (ZnP-DOPE), in which DOPE represents 1,2-Dioleoyl-*sn*-glycero-3-phosphoethanolamine. Electrochemical impedance analysis of these films reveals hybrid structures that conform with a bilayer model[9,22] (Figure 2 and Table 1), confirming that monolayer quantities of lipids can be deposited on a fluorinated alkanethiol SAM similar to those based on *n*-alkanethiols as previously reported.[23] Additional measurements from a quartz crystal microbalance and from UV/Vis spectroscopy for these hybrid bilayers further indicate that the top 1-palmitoyl-2-oleoyl-sn-glycero-3-phosphocholine (POPC) monolayers formed on the two SAMs exhibit comparable lipid loading and packing density (see the Supporting Information Figures S1 and S2).

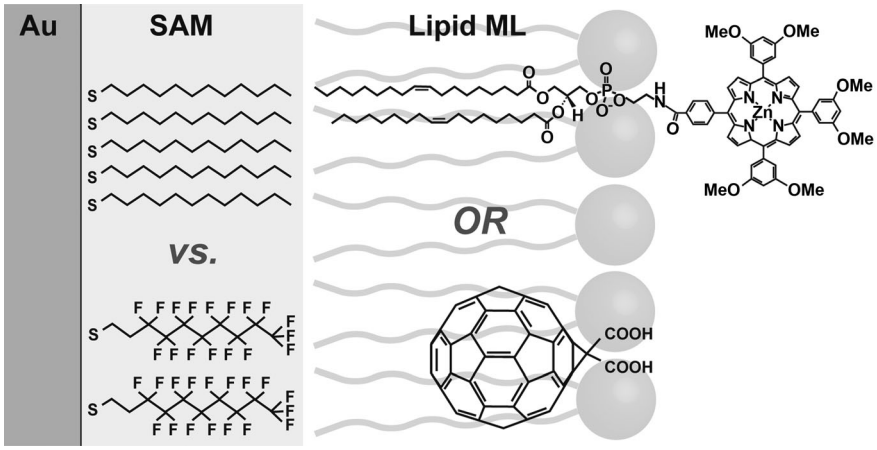

Figure 1. Presentation of the photovoltaic model based on alkanethiol/lipid hybrid bilayers. The bilayers comprise a SAM of either dodecanethiol ($C_{12}H_{25}SH$) or heptadecafluoro-1-decanethiol ($C_{10}F_{17}SH$) and an upper POPC lipid monolayer assembled with either zinc porphyrin (ZnP) or malonic fullerene (C_{63}). Chemical structures are not drawn to scale with each other.

2.2 Photovoltaic Behaviors of Hybrid-Bilayer-Based Photocells

Figure 3a compares the anodic/cathodic photocurrents obtained from hybrid bilayers that contain a concentration of 2 mol% ZnP-DOPE in the top POPC layer. As discussed in our previous work,[10] these photocurrents result from photoinduced electron-transfer processes between excited porphyrin and sacrificial redox agents in solution. Here in the anodic process, a photocurrent of approximately 130 nA cm^{-2} was gener-

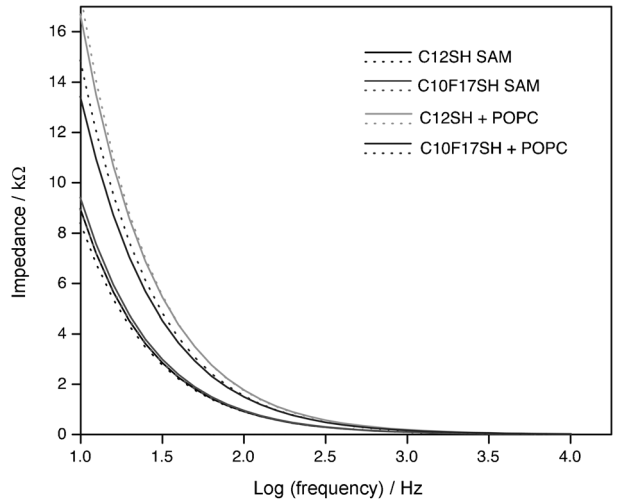

Figure 2. Impedance profile of SAMs and hybrid bilayers as a function of the applied alternating current frequency. The supporting electrolytes contain KCl (10 mM) in deionized water. Dotted lines are fitting results based on a series resistor-capacitor circuit model. See the Experimental Section for more details.

Table 1. Capacitance and calculated dielectric thickness values of SAMs and lipid layers.

SAM	C_{SAM}[a] [μF cm^{-2}]	d_{SAM}[b] [Å]	C_{BL}[c] [μF cm^{-2}]	C_{lipid}[d] [μF cm^{-2}]	d_{lipid}[e] [Å]
$C_{12}H_{25}SH$	1.51 ± 0.004	13.5	0.90 ± 0.01	2.25	10.6
$C_{10}F_{17}SH$	1.53 ± 0.01	12.2	0.92 ± 0.05	2.30	10.4

[a] Capacitance of SAM layer. [b] Dielectric thickness of SAM layer. [c] Capacitance of the bilayer. [d] Capacitance of the lipid layer. [e] Dielectric thickness of lipid layer.

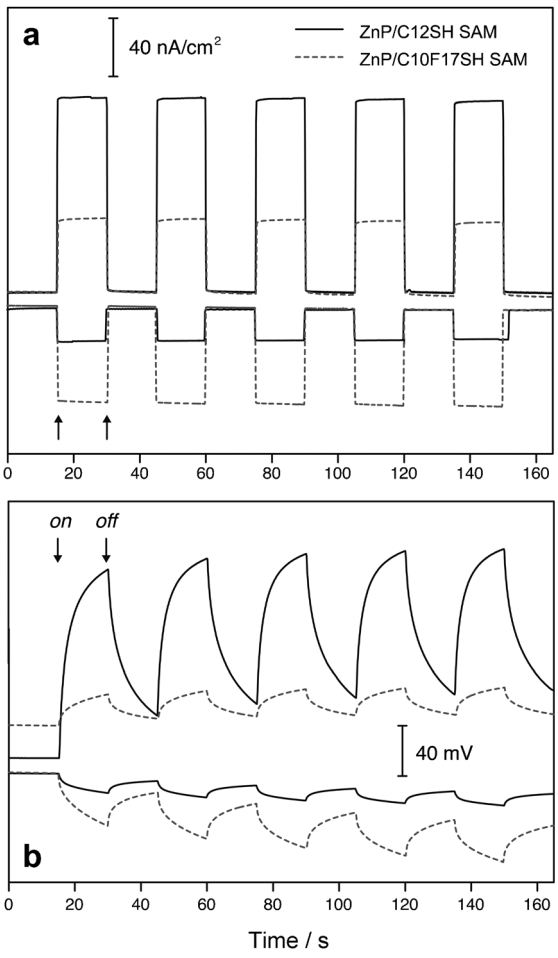

Figure 3. Photocurrent (a) and photovoltage (b) signals generated from ZnP-DOPE (2%) in POPC lipid monolayers on either $C_{12}H_{25}SH$ SAM (——) or $C_{10}F_{17}SH$ SAM (-----). The anodic photocurrents (upward traces) were generated in ascorbate (50 mM, sacrificial electron donor) dissolved in HEPES buffer (10 mM HEPES, 100 mM Na_2SO_4, pH 7.7), in which oxygen was depleted by adding glucose (50 mM), glucose oxidase (50 units mL^{-1}), and catalase (200 units mL^{-1}), whereas the cathodic photocurrents (downward traces) were obtained from methyl viologen (50 mM, primary electron acceptor) dissolved in the same buffer. All photocurrents were collected with the three-electrode electrochemical cell as described in the Experimental Section; the excitation light was provided by a Hg lamp filtered at 417 ± 30 nm with an average intensity of 40 mW cm^{-2}. Arrows indicate the times the light is turned on/off.

ated from the bilayers with the C_{12} SAM as the underlayer, whereas a lower current of approximately 50 nA cm^{-2} was obtained if the underlying SAM was $C_{10}F_{17}SH$ instead. The difference in the anodic currents does not owe to different loadings of ZnP-DOPE on the two SAMs during the hybrid bilayer formation, as an opposite trend was seen from the cathodic photocurrents obtained from the same devices (dashed traces, Figure 3a). These responses indicate the photocurrent generation process is instantaneous and relatively stable in these devices. The photovoltages recorded from devices subject to similar dark/light cycles display a similar trend, that is, higher voltage amplitudes accompanying higher currents and vice versa (Figure 3b). Unlike the photocurrents, the photovoltages increase only gradually upon photoexcitation and cannot reach steady states in a given light on/off cycle (t = 15 s). This sluggish behavior reflects the dynamic response of the charging/discharging processes of this bilayer-based photoelectrochemical system under photoexcitation. In particular, the relatively steep rise in photovoltage as the light is just turned on reflects the fast initial accumulation of charges around the bilayer as a result of photoinduced electron transfer; as such a process continuously charges up the bilayer, the latter approaches its capacity, causing further charging to slow down.

If bilayers that contain C_{63} (2 mol%) in the top POPC layer are subjected to similar photocurrent/photovoltage generation, a similar, although less marked, trend is observed (Figure 4). A lower anodic current (i.e. 60 vs 85 nA cm^{-2}) and a higher cathodic current (i.e. 18 vs 10 nA cm^{-2}) is obtained if $C_{10}F_{17}SH$ SAMs replace C_{12} SAMs as the underlying layer in the bilayers. Photovoltages again follow photocurrents. In all cases, bilayer cells with no photoagents included only produced negligible currents (not shown).

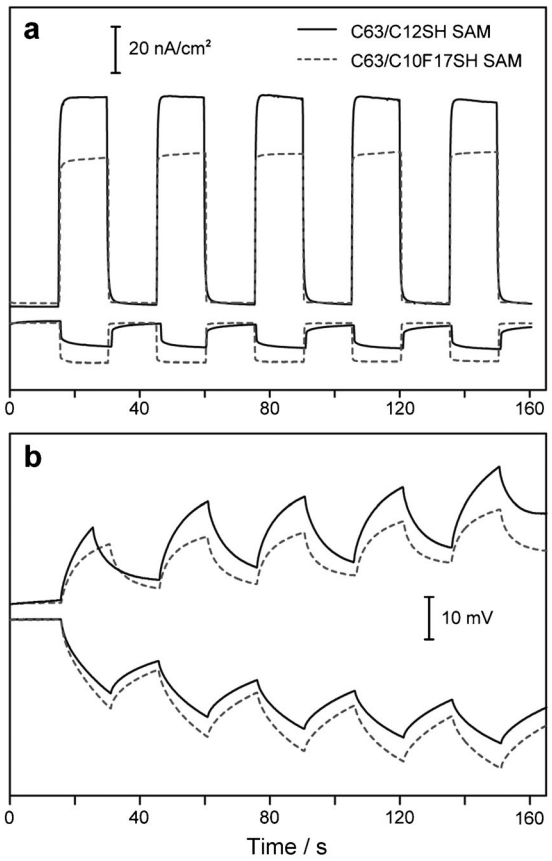

Figure 4. Photocurrent (a) and photovoltage (b) responses obtained from fullerene C_{63} (2%) assembled in POPC lipid monolayers on either $C_{12}H_{25}SH$ SAM (——) or $C_{10}F_{17}SH$ SAM (-----). The anodic photocurrents are presented as upward traces and the cathodic photocurrents by downward traces. All other conditions are identical to those in Figure 3.

2.3 Mechanisms of Photocurrent/Photovoltage Modulation: Considerations Regarding the Organization of Photoagents in the Lipid Monolayer

To account for the modulated photovoltaic behaviors of lipid-assembled photoagents by the underlying SAMs, we next consider the organization, position and orientation of these two agents in the bilayers. In terms of organization, the ZnP complex is directly linked to DOPE by the amine headgroup, whereas fullerenes are incorporated into lipids non-covalently. As such, the porphyrin moieties are expected to take position at the top of the lipid monolayer surface upon lipid fusion on the SAMs. Conversely, the malonic group on fullerene C_{63} renders amphiphicity to the sphere-shaped molecule, which should position itself relatively snugly within the surrounding amphiphilic lipids, so that the exposure of its hydrophobic bulk (/polar malonic group) to water (/lipid acyl chains) can be simultaneously minimized. Thus, fullerene C_{63} is located closer to the SAM and the gold surface compared to ZnP in a hybrid bilayer.

So just how deeply is the malonic fullerene embedded in the POPC monolayer and how close is it to the underlying SAM? To answer these questions, we evaluate its size and position in relation to the thickness of the POPC monolayer. First of all, the spherical fullerene tends to avoid space immediately below the carbonyls of the lipids, that is, the space occupied by the uppermost methylene groups in the acyl chains, because its bulky size would otherwise increase the interspatial distance between the lipids and thus break the balance of various forces[24] that stabilize the lipid/water interface. To minimize such an energy penalty, the fullerene preferentially takes positions about midway of the lipid hydrocarbon region.[25] This picture also holds true for singly modified fullerenes. For example, Bortolus et al.[26] have found that several singly region-derivatized fullerenes tend to occupy spaces below the lipid/water interface in the lipid matrix, similar to C_{60}. On the other hand, the hydrophobic thickness of POPC bilayers has been determined to be 25.8 Å by NMR[27] and 27.1 Å by X-ray scattering.[28] Assuming the thickness of the POPC monolayer remains the same in a hybrid bilayer configuration, it follows that the bottom edge of the POPC-assembled fullerene (diameter of $\approx$10 Å) should be fairly close to the hydrocarbon end of the lipid monolayer (i.e. the left edge of C_{60} within 3–4 Å to the SAMs on the far left in Figure 1). The highly disordered nature of the liquid-crystalline POPC matrix, as well as the likely site distribution of the assembled occupants, may further shorten this gap.

2.4. Mechanisms of Photocurrent/Photovoltage Modulation: Dipole Potentials Contributed by the Lipid Monolayer and SAMs

The observed modulation effects clearly arise from the different physiochemical characteristics built into the two hybrid-bilayer-based matrices. In this section, we evaluate how and to what extent each layer can modify the effective energy levels of the two photoagents. For the upper layer, it is understood that several membrane-associated electrostatic potentials will develop as lipids assemble to form monolayers and bilayers at water/organic or water/water interfaces. Of particular importance here is the so-called membrane dipole potential,[29–31] which is formed between the lipid polar headgroups and the low-dielectric hydrocarbon chains by aligned dipoles of the lipid headgroup moieties; these include choline, phosphate and carbonyl, as well as the hydration water molecules surrounding these groups. This dipole potential is largely attributed to the oriented water molecules that organized at/near the lipid/water interface because the choline(+)-phosphate(−) dipoles are found to be oriented almost parallel to the monolayer/bilayer surface[32] and the headgroup charges are overcompensated by the water molecules.[33] As determined by voltage-sensitive dye fluorescence measurements,[30,34] this typically results in a potential of approximately 200 mVs across a zwitterionic POPC monolayer, with water as the negative side. Considering the assembled position of the two photoagents in the lipid monolayer, one finds that the DOPE-conjugated ZnP moieties occupy little space in the hydrocarbon region of the lipid matrix, in which the most significant dipole potential drop develops. By contrast, the lipid-assembled fullerenes reside right in this dipole-active zone owing to their penetration into the hydrocarbon region of the lipid matrix. Since the

electric field associated with a dipole layer is extremely localized (normally dropping to zero a few Ångström away from the initiating layer),[35] the different positions occupied by the two photoagents critically determine whether and to what extent the membrane dipole can shift their respective energy levels. Moreover, since the modulated photoelectrochemical responses result from charge transfer processes occurring between the space of photoagents and the gold electrode, only dipoles situated in between these two layers are expected to directly impact these processes. This leads us to conclude that the lipid associated dipole only plays a minor role in modifying the energetics in fullerene-based devices, as it lies at the outside of the assembled fullerenes. Whereas for the ZnP-containing cells, the same membrane dipole sits right within the confinement of the electrode and lipid headgroups and therefore, a dipole potential of 0.2 eV is specifically included in this case (vide infra).

Similarly, it can be expected that the dipole potential contributions of the underlying SAMs would modify the interfacial energetics. Specifically, the more electronegative sulfur atom in the C_{12} thiol pulls electron density away from the adjacent methylene groups, forming a dipole with the sulfur as the negative pole; the opposite is true for $C_{10}F_{17}SH$, in which the electron clouds are pulled towards the distal fluorinated side of the molecule. This is further shown by the calculated dipole moments[36] of the two adsorbates: 1.79 D for the C_{12} thiol and −1.28 D for $C_{10}F_{17}SH$. Upon formation of self-assembled monolayers on gold, these polar molecules will yield a collective dipole that contains a non-zero component normal to the gold surfaces.

2.5. Mechanisms of Photocurrent/Photovoltage Modulation: A Combined Analysis

We then combined the two sources of dipole potentials in a more quantitative analysis of the overall cell energetics. For devices governed by tunneling-based charge injection processes, the efficiency of hole (/electron) injection can be significantly influenced by the energy differences between the Fermi potential level of the electrode and the HOMO(/LUMO) level, respectively, of the organic semiconductor immobilized on top of the electrode, that is, the hole/electron injection barriers.[3,38] As discussed in the Introduction, one exploitable strategy of minimizing the charge injection barriers and thus enhancing the injection efficiency is by using a dipole layer to interface the organic material and the electrode. Depending on its dipole orientation relative to the electrode, the dipole layer acts to shift up (or down) the effective vacuum energy level, which makes the removal of electrons from the metal more (or less) energetically costly, resulting in an increase (or a decrease) in the work function of the metal. If the same process additionally involves an organic (photoagent) layer at the outside, the HOMO/LUMO levels of the latter can be shifted by the inserted dipole layer as well, because it shares a common effective vacuum level with the gold substrate during the charge injection process.[38]

Following solid-state physics convention, the HOMO energy of ZnP is estimated from its first oxidation potential[39] and converted to absolute scale (5.6 eV) versus the vacuum [i.e. potential of the latter is taken as 4.5 eV[40] vs the normal hydrogen electrode (NHE)]. Its LUMO level, 3.5 eV, is estimated from the Weller relationship: $E_{LUMO} = E_{HOMO} - \Delta E_{0,0}$, in which $\Delta E_{0,0}$ is the $0 \rightarrow 0$ transition energy of ZnP (i.e. ≈ 2.1 eV as determined from ZnP fluorescence emission spectrum, Figure S3). A value of 4.9 eV is used as the work function of gold under ambient conditions.[41] In the case of dipole potentials rendered by alkanethiol SAMs, Kelvin probe measurements[41] by de Boer et al. determined that $C_{10}F_{17}SH$ SAM could increase the work function of gold by 0.6 eV relative to the unmodified gold, whereas the oppositely polarized C_{16} alkanethiol effectively lowered the gold work function by 0.8 eV. These values,[42] together with the contribution from the lipid membrane dipole, are taken into the analysis of energetics responsible for ZnP-based bilayer cells (Figure 5). As shown in Figure 5b, the dipole associated with the C_{12} SAM lowers the HOMO/LUMO levels of ZnP versus the vacuum, which is partially counteracted by the lipid dipole that points to the opposite direction. In consequence, its effective LUMO level (4.1 eV) is now more closely aligned with the Fermi level of gold ($E_F = 4.9$ eV), whereas the gap between its HOMO and the gold Fermi level is enlarged. These changes accordingly produce an electron-injection barrier (EIB) of 0.8 eV and a hole-injection barrier (HIB) of 1.3 eV in thus-prepared bilayer devices. By contrast, the effective energy levels associated with ZnP will be increased if $C_{10}F_{17}SH$ is used to form the bilayers, which result in a very small HIB (0.1 eV) and a very large EIB (2.2 eV), as shown in Figure 5c. Together, the dipole potentials from SAMs and lipids in these hybrid bilayers modify the thermodynamic barrier for charge injection to occur, which leads to a more efficient anodic photovoltaic process (owing to a small EIB) in the case of C_{12} thiol and a facile cathodic process (owing to a small HIB) for the fluorinated thiol as shown in Figure 3.

Similar energy diagrams for C_{63}-based devices can be sketched by putting together the respective potential energy levels of each participating component (Figure 6). As discussed above, the contribution from the lipid membrane dipole in the overall energetics is expected to be small because of its small overlap with the charge-injection path. Hence, a maximal anodic photocurrent can be predicted for the C_{12} SAM-based cells as the estimated EIB is zero, that is, the LUMO of assembled $C_{63} = 4.1 - (-0.8, C_{12}\ SAM) = 4.9$ eV, whereas a higher cathodic generation is expected for the $C_{10}F_{17}SH$-based cells due to a lower HIB. These estimates again agree with experimental data shown in Figure 4.

Although a similar trend is shared by the two photoagents investigated here, the level of modulation is noticeably smaller in the fullerene-based devices. For example, the anodic photocurrents obtained from fullerenes assembled on the two SAMs differ only by approximately 30%, despite the fact that their EIBs are estimated to be 1.4 eV apart. The relatively weak modulation of fullerene-based cells is probably due to their location in the bilayer as well as their high molecular polarizability (e.g. the ground-state polarizability[43] of C_{60} is 84 Å^3). Assem-

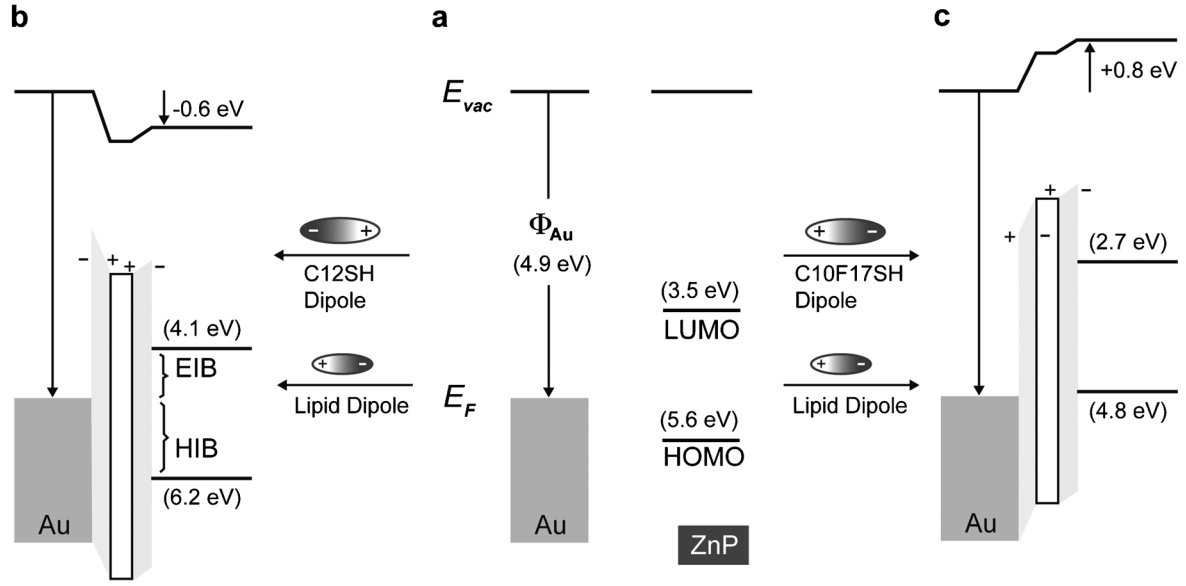

Figure 5. Energy diagrams of ZnP-based photovoltaic systems. In panel a) the gold Fermi energy level (E_F) and the HOMO/LUMO levels of ZnP are separated in vacuum. b) Lowering of HOMO/LUMO levels of ZnP versus E_F(Au) induced by the dipole of $C_{12}H_{25}SH$ SAM situated in between the electrode and the photoagent. c) Upshifting of HOMO/LUMO levels of ZnP versus E_F(Au) induced by the dipole of $C_{10}F_{17}SH$ SAM situated in between the electrode and the photoagent. In both configurations, a 0.2 eV contributed by the lipid membrane dipoles is included.

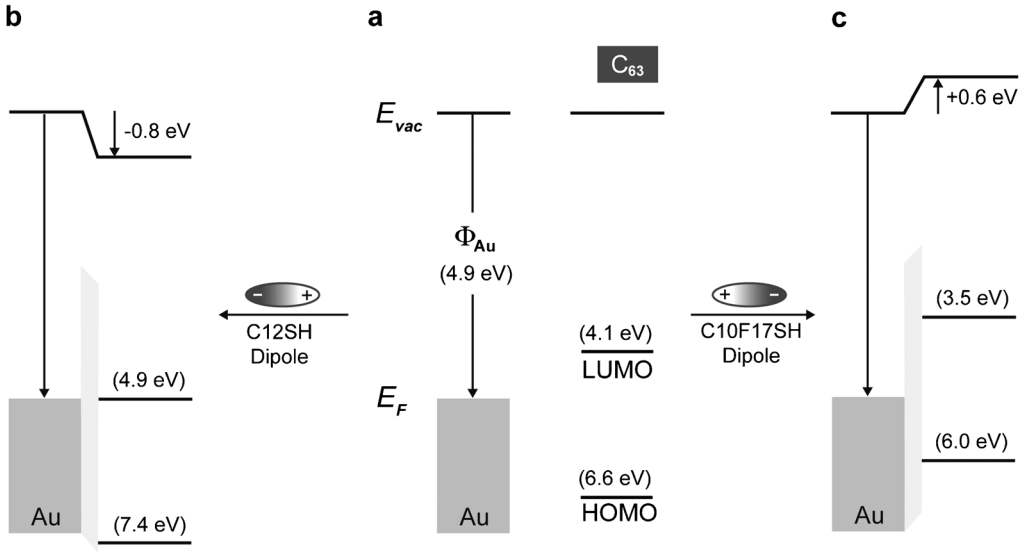

Figure 6. Energy diagrams of C_{63}-based photovoltaic systems. In panel a) the gold Fermi energy level (E_F) and the HOMO/LUMO levels of fullerene C_{63} are separated in vacuum. b) Shifting of HOMO/LUMO levels of C_{63} versus E_F(Au) by the dipole of $C_{12}H_{25}SH$ SAM. c) Shifting of HOMO/LUMO levels of C_{63} versus E_F(Au) by the dipole of $C_{10}F_{17}SH$ SAM.

bled as such, the polarizable molecule framework of fullerene may directly experience the surrounding dipoles and electronically dampen the polarization imposed by the latter, which gives rise to a weakened modulation. In a sense, this counteracting effect bears similarity with the depolarization effect seen in the SAM formation on a substrate,[35] in which individual adsorbates only display a dipole less than their gas-phase value as the result of a compensating electric field, which originates between the substrate and the SAM pointing in the opposite direction. Consequently, this depolarization effect may pose a limit on the achievable modification of charge-injection barriers with polar SAMs in fullerene-based OPV systems. Follow-up computational studies of the present system may lead to more insights into the mechanism and control of such an effect in the near future.

3. Conclusions

We have found that the intrinsic dipoles of lipids and alkanethiols can be used to modulate photoinduced charge-injection processes in alkanethiol/lipid-based bilayer photovoltaic systems. These modulation effects are satisfactorily explained by

dipole-induced modification of the work functions of the metal substrates and hence the Shockley energy barriers; a concept well established and broadly exploited in organic LEDs and field-effect transistors.[12,19,35,38] Our results reveal the intricacy of an orientated surface dipole in influencing photovoltaic processes, and its subtle interplay with other related factors, such as the polarizability, location and orientation of the photoagents. These findings clearly point to the potential of controlling and designing electronic and dielectric properties of thin-film-based photovoltaic and organoelectronic systems by using self-assembled structures.

Experimental Section

Chemicals

Phospholipids such as 1-palmitoyl-2-oleoyl-*sn*-glycero-3-phosphocholine (POPC) and 1,2-dioleoyl-*sn*-glycero-phosphoethanolamine (DOPE) were received from Avanti Polar Lipids with purity >99%. Monomalonic fullerenes (C_{63}) were prepared according to previously reported procedures.[8] Dodecanethiol, 1H,1H,2H,2H-perfluorodecanethiol ($CF_3(CF_2)_7(CH_2)_2SH$), 4-(2-hydroxyethyl) piperazine-1-ethanesulfonic acid (HEPES), methyl viologen dichloride hydrate (MV^{2+}), L(+)-ascorbic acid sodium salt, D-(+)-glucose, glucose oxidase (type X-S from *Aspergillus niger*) and catalase from bovine liver were obtained from Sigma–Aldrich. All chemicals received were of the highest grade available. All solutions were prepared with 18.2 MΩ cm^{-1} deionized water (Millipore).

Synthesis of 5-(4-carboxyphenyl)-10,15,20-tri-(3,5-dimethoxyphenyl)porphyrin (2)

The monoacid porphyrin was synthesized according to a slightly modified literature procedure.[44] Pyrrole (12 mmol, 4 equiv.), 3,5-dimethoxybenzaldehyde (9 mmol, 3 equiv.), and 4-methyl-carboxybenzaldehyde (3 mmol, 1 equiv.) were dissolved in chloroform (300 mL) and stirred under nitrogen for 5 min. Then $BF_3{\cdot}OEt_2$ (0.9 mmol, 0.3 equiv., 46%) was added, and the reaction was stirred for 7 h. *p*-Chloranil (2 equiv.) was added to the reaction mixture in one portion, and the solution was stirred for an additional 4 h. After completion of oxidation (monitored by TLC), the mixture was filtered through a short pad of SiO_2 into the desired monoester porphyrin together with other porphyrins (900 mg). The mixed porphyrins (240 mg) were dissolved in THF (24 mL), and KOH (2 M, 15 mL) was added. The solution was heated at reflux for 12 h and cooled to RT, acidified with 10% HCl, and the THF was removed under reduced pressure. The remaining aqueous phase was extracted with dichloromethane (3×100 mL). The organic extracts were combined, washed with water and dried with anhydrous Na_2SO_4. The solvent was removed under vacuum and the residue was purified by column chromatography (10% MeOH in DCM) to give the pure monoacid **2** (110 mg). ^{1}H NMR (400 MHz, $CDCl_3$): δ = 8.98 (d, J = 4.8 Hz, 2H), 8.95 (s, 4H), 8.80 (d, J = 4.8 Hz, 2H), 8.54 (d, J = 7.8 Hz, 2H), 8.35 (d, J = 8.0 Hz, 2H), 7.41 (m, 6H), 6.91 (s, 3H), 3.97 (s, 18H), −2.80 ppm (s, 2H); ^{13}C NMR (62.5 MHz, $CDCl_3$): δ = 169.66, 158.94, 143.99, 134.78, 131.51, 128.68, 120.21, 113.99, 100.25, 55.73 ppm. UV/Vis ($CHCl_3$): λ_{max} nm (log ε) = 420 (5.50), 515 (4.26), 550 (3.94), 595 (3.78), 645 (3.61). HRMS (ESI): ($[M+H]^+$) calcd for $C_{51}H_{42}N_4O_8{\cdot}H^+$: 839.3081; found: 839.3093.

Synthesis of 5-(4-Carboxyphenyl)-10,15,20-tris-(3,5,di-methoxyphenyl)porphyrin zinc complex (1)

N,*N*-dimethylformamide (2.5 mL) and zinc(II) acetate (18 mg, 0.10 mmol) were added to porphyrin carboxylic acid **2** (8.5 mg, 0.010 mmol). The solution was heated to T = 60 °C and allowed to stir overnight. The solvent was then removed under reduced pressure and the residue was extracted with methylene chloride (2× 10 mL) and water. The organic layers were combined, dried with magnesium sulfate, filtered, and concentrated. *N*,*N*-dimethylformamide (1 mL), hydroxybenzotriazole (HOBt, 1 mg, 0.007 mmol), *O*-benzotriazole-*N*,*N*,*N*′,*N*′-tetramethyl-uronium hexaflurophosphate (HBTU, 4 mg, 0.010 mmol), and *N*,*N*-diisopropylethylamine (DIEA, 3.3 μL, 0.020 mmol) were added to the crude product. A solution of dioleylphosphatidylethanolamine (DOPE, 5 mg, 0.0067 mmol) in chloroform (1 mL) was added to the reaction mixture and the reaction was allowed to stir at RT overnight. The solvent was removed and the solution was purified by chromatography on silica gel with a gradient of methanol-methylene chloride (0–10%). The resulting porphyrin-lipid conjugate (**1**) was obtained as a purple solid (9.5 mg, 61%). ^{1}H NMR (300 MHz, $CDCl_3$:CD_3OD): δ = 8.96 (s, 6H), 8.79 (d, J = 6 Hz, 2H), 8.33–8.24 (m, 4H), 7.42–7.40 (m, 6H), 6.91–6.88 (m, 3H), 5.32–5.24 (m, 4H), 4.24–4.15 (m, 3H), 4.10–4.03 (m, 1H), 3.97–3.95 (m, 22H), 3.86–3.80 (m, 4H), 3.68–3.65 (m, 1H), 2.36–2.26 (m, 4H), 2.03–1.91 (m, 8H), 1.63–1.53 (m, 4H), 1.27–1.23 (m, 40H), 0.87–0.83 ppm (m, 6H); ^{31}P NMR (121.5 MHz, $CDCl_3$:CD_3OD): δ = 2.02 ppm (s, 1P). HRMS [M+2H] calcd:1627.7654; found: 1627.4823.

Computation

Dipole moments of the thiols were calculated with ab initio and density functional theory (DFT) techniques by using Gaussian 09[45]/GaussView 5. To start, the geometry of the two thiols was first optimized at Hartree–Fock level by the STO-3G basis set and the energy of the geometry-optimized molecules (or their neutral radicals in which the hydrogen atom attached to the sulfur atom is removed) was then calculated with DFT at the B3LYP/6-31G(2d,2p) level.

Preparation of SAMs and HBMs

The formation of SAMs on gold substrates was accomplished by immersing gold-coated substrates in an ethanol solution (1 mM) of alkanethiols at RT for at least 15 h. Prior to this step, the gold-coated substrates were thoroughly cleaned in piranha solution (3:1, concentrated H_2SO_4 to 30% H_2O_2 solution, *v*/*v*) for 15 min, and rinsed with water and ethanol and dried by an argon stream. The SAM-modified gold substrates were carefully rinsed with ethanol and deionized water, dried in argon, and immediately assembled in homemade Teflon cells to be used either for impedance analysis or photoelectrochemical measurements. Preparation of liposome samples that contained fullerenes[8] or porphyrin-conjugated lipids[10] has been reported previously. Briefly, POPC and either of the photoagents (2 mol%) were mixed in chloroform and thoroughly dried. The resulting lipid films were re-suspended in 4-(2-hydroxyethyl)-1-piperazineethanesulfonic acid (HEPES, 10 mM) buffer saline (0.1 M NaCl, pH 7.7) to give final solutions of POPC (2.5 mM). Liposome solutions of these precursors were prepared by extruding the corresponding suspensions consecutively through porous polycarbonate membranes with average pore diameters of 400 and 80 nm. Aliquots (0.3 mL) of these solutions were typically added to the cell and incubated for 2 h to form lipid/alkanethiol hybrid bilayers. The unbound vesicle solutions in the cells were re-

placed by the same HEPES buffer solution before performing further measurements.

UV/Vis and Fluorescence Spectroscopy

UV/Vis spectra were acquired with a UV/Vis spectrophotometer (Cary 50 Bio, Varian) and the fluorescence emission spectra of ZnP-DOPE in liposome were collected on a Shimadzu RF-5301 fluorospectrometer. A home-made Teflon cell was fitted to the sample holder of the spectrometer and optically aligned to obtain absorption spectra of chlorophyll α assembled in hybrid bilayers. The cell was configured to have an all-through liquid reservoir that could be sandwiched between two planar substrates, one of which was a semi-transparent gold substrate (10 nm Au coated on glass slides, Sigma–Aldrich) and the other was microscope cover slides.

Quartz Crystal Microbalance (QCM)

QCM measurements were performed on a QCM analyzer equipped with a 5 MHz crystal oscillator (Model QCM25, Stanford Research Systems) similar to a previous report.[9] Clean gold-coated quartz crystal disks were incubated in ethanol solutions of thiols ($C_{12}H_{25}SH$ or Fc-$C_{11}H_{24}SH$, 1 mM) at RT for at least 15 h and then rinsed with ethanol and deionized water, and dried in argon. These SAM-covered quartz disks were then mounted onto the QCM oscillator connected to a flow cell. HEPES buffer (10 mM HEPES, 100 mM Na_2SO_4, pH 7.7) was first flowed through the cell until a steady frequency baseline was obtained (i.e. $\Delta f < 1.0$ Hz over 10 min). POPC liposome solutions of approximately 0.15 mM total lipids were pumped into the cells to form hybrid bilayers.

Impedance Spectroscopy

Impedance spectroscopy measurements of the alkanethiol SAMs and corresponding alkanethiol/lipid hybrid bilayers were conducted on a Gamry electrochemical impedance analyzer system (Reference 600). Homemade Teflon cells used herein contained a film-modified Au working electrode (effective area: ≈ 1.13 cm^2), a Ag/AgCl reference electrode and a Pt counter electrode immersed in KCl aqueous solution (10 mM). During the impedance measurements, the electrochemical cells were biased with a 10 mV alternating current voltage operated in the frequency range from 10 to 10 kHz. The obtained impedance data were fitted to a series resistor–capacitor circuit model by using a modeling package included in Gamry Echem Analyst. These fits directly gave capacitance values of SAMs and hybrid bilayers, whereas that of the lipid monolayer was calculated by using equation: $C_{lipid}^{-1} = C_{BL}^{-1} - C_{SAM}^{-1}$, in which C is the capacitance. The thicknesses of each of the layers was then calculated by using the following relationship: $1/C = d/\varepsilon\varepsilon_0$, in which d is the thickness of the dielectric medium that separates the two conducting plates (i.e. the gold electrode and the electrolyte solution), ε is the dielectric constant of the separating medium (i.e. 2.3 for $C_{12}SH$, 2.1 for $C_{10}F_{17}SH$ and 2.7 for POPC), and ε_0 is the permittivity of free space ($\varepsilon_0 \approx 8.854 \times 10^{-12}$ F m^{-1}). Standard deviations were obtained from four measurements.

Electrochemical and Photoelectrochemical Measurements

Electrochemical and photoelectrochemical measurements were performed with a potentiostat (CHI 910B, CH Instruments) in the aforementioned Teflon cells that housed three electrodes. Photocurrents were measured amperometrically with potentials set equal to the open circuit potential of each cells determined separately under dark conditions; whereas photovoltages were acquired in the open-circuit potential mode. In both measurements, the cells were irradiated with light from an Hg lamp (X-Cite, series 120 PC, EXFO) filtered at 417 ± 30 nm (average intensity: 40.0 mW cm^{-2}). An ascorbate (50 mM) in HEPES buffer (10 mM HEPES, 100 mM NaCl or Na_2SO_4, pH 7.7) was used as the sacrificial electron donor in the anodic generation; oxygen was removed from the cells by adding glucose (50 mM), glucose oxidase (50 units mL^{-1}), and catalase (200 units mL^{-1}) to the solutions. Under cathodic conditions, the un-deaerated electrolyte solutions contained methyl viologen (50 mM) and Na_2SO_4 (100 mM) in HEPES buffer.

Acknowledgements

This work is supported by the National Science Foundation (award No.: CHE-0951743 to W.Z., CHE-0954297 to M.D.B., and CHE-1152767 to X.P.Z.). X.P.Z. also acknowledges support from the King Abdullah University of Science and Technology (KAUST) (Award FIC/2010/06). Computation in this work was carried out using facilities at the Alabama Supercomputer Center. W.Z. thanks Dr. O. Acevedo (AU) for providing software for calculation.

Keywords: charge-carrier injection · electrochemistry · lipids · magnetic properties · self-assembly

[1] B. Kippelen, J.-L. Bredas, *Energy Environ. Sci.* **2009**, *2*, 251 – 261.
[2] M. Graetzel, R. A. J. Janssen, D. B. Mitzi, E. H. Sargent, *Nature* **2012**, *488*, 304 – 312.
[3] G. Heimel, L. Romaner, E. Zojer, J.-L. Bredas, *Acc. Chem. Res.* **2008**, *41*, 721 – 729.
[4] D. Beljonne, J. Cornil, L. Muccioli, C. Zannoni, J.-L. Bredas, F. Castet, *Chem. Mater.* **2011**, *23*, 591 – 609.
[5] H. Imahori, Y. Mori, Y. Matano, *J. Photochem. Photobiol. C* **2003**, *4*, 51 – 83.
[6] T. Konishi, A. Ikeda, S. Shinkai, *Tetrahedron* **2005**, *61*, 4881 – 4899.
[7] T. Kondo, K. Uosaki, *J. Photochem. Photobiol. C* **2007**, *8*, 1 – 17.
[8] W. Zhan, K. Jiang, *Langmuir* **2008**, *24*, 13258 – 13261.
[9] K. Jiang, H. Xie, W. Zhan, *Langmuir* **2009**, *25*, 11129 – 11136.
[10] W. Zhan, K. Jiang, M. D. Smith, H. E. Bostic, M. D. Best, M. L. Auad, J. V. Ruppel, C. Kim, X. P. Zhang, *Langmuir* **2010**, *26*, 15671 – 15679.
[11] H. Xie, K. Jiang, W. Zhan, *Phys. Chem. Chem. Phys.* **2011**, *13*, 17712 – 17721.
[12] K. C. Kao, *Dielectric Phenomena in Solids*, Elsevier Academic Press, San Diego, **2004**, Chap. 6.
[13] H. E. Ives, A. R. Olpin, *Phys. Rev.* **1929**, *34*, 117 – 128.
[14] J. J. Brady, *Phys. Rev.* **1932**, *41*, 613 – 626.
[15] J. Bardeen, *Phys. Rev.* **1936**, *49*, 653 – 663.
[16] I. H. Campbell, S. Rubin, T. A. Zawodzinski, J. D. Kress, R. L. Martin, D. L. Smith, N. N. Barashkov, J. P. Ferraris, *Phys. Rev. B* **1996**, *54*, R14321 – R14324.
[17] D. M. Alloway, M. Hofmann, D. L. Smith, N. E. Gruhn, A. L. Graham, R., Jr. Colorado, V. H. Wysocki, T. R. Lee, P. A. Lee, N. R. Armstrong, *J. Phys. Chem. B* **2003**, *107*, 11690 – 11699.
[18] R. T. Tung, *Mater. Sci. Eng. R* **2001**, *35*, 1 – 138.
[19] S. Braun, W. R. Salaneck, M. Fahlman, *Adv. Mater.* **2009**, *21*, 1450 – 1472.
[20] V. D. Mihailetchi, L. J. A. Koster, P. W. M. Blom, C. Melzer, B. de Boer, J. K. J. van Duren, R. A. J. Janssen, *Adv. Funct. Mater.* **2005**, *15*, 795 – 801.
[21] J. Kim, D.-Y. Khang, J.-H. Kim, H. H. Lee, *Appl. Phys. Lett.* **2008**, *92*, 133307.
[22] A. L. Plant, *Langmuir* **1993**, *9*, 2764 – 2767.
[23] V. I. Silin, H. Wieder, J. T. Woodward, G. Valincius, A. Offenhausser, A. L. Plant, *J. Am. Chem. Soc.* **2002**, *124*, 14676 – 14683.
[24] J. N. Israelachvili, *Intermolecular and Surface Forces, 3rd ed.*, Elsevier, Amsterdam, **2011**.

[25] L. Li, H. Davande, D. Bedrov, G. D. Smith, *J. Phys. Chem. B* **2007**, *111*, 4067 – 4072.
[26] M. Bortolus, G. Parisio, A. L. Maniero, A. Ferrarini, *Langmuir* **2011**, *27*, 12560 – 12568.
[27] F. A. Nezil, M. Bloom, *Biophys. J.* **1992**, *61*, 1176 – 1183.
[28] N. Kucerka, S. Tristram-Nagle, J. F. Nagle, *J. Membr. Biol.* **2005**, *208*, 193 – 202.
[29] H. Brockman, *Chem. Phys. Lipids* **1994**, *73*, 57 – 79.
[30] R.. Clarke, *Adv. Colloid Interface Sci.* **2001**, *89*, 263 – 281.
[31] A. P. Demchenko, S. O. Yesylevskyy, *Chem. Phys. Lipids* **2009**, *160*, 63 – 84.
[32] H. Hauser, I. Pascher, R. H. Pearson, S. Sundell, *Biochim. Biophys. Acta* **1981**, *650*, 21 – 51.
[33] K. Gawrisch, D. Ruston, J. Zimmerberg, V. A. Parsegian, R. P. Rand, N. Fuller, *Biophys. J.* **1992**, *61*, 1213 – 1223.
[34] R. J. Clarke, *Biochim. Biophys. Acta Biomembr.* **1997**, *1327*, 269 – 278.
[35] A. Natan, L. Kronik, H. Haick, R. T. Tung, *Adv. Mater.* **2007**, *19*, 4103 – 4117.
[36] Calculations were also performed on the neutral radicals of the two thiols using procedures similar to refs. [16, 17], which give 2.00 D for $C_{12}H_{25}SH$ and −0.91 D for $C_{10}F_{17}SH$. Dipole calculations based on these neutral radicals are known to underestimate the contributions of the Au–S bond to the overall dipole of the gold-attached thiol molecules[37] but are expected to produce the correct trend in our case.
[37] L. J. Wang, G. M. Rangger, Z. Y. Ma, Q. K. Li, Z. Shuai, E. Zojer, G. Heimel, *Phys. Chem. Chem. Phys.* **2010**, *12*, 4287 – 4290.
[38] H. Ishii, K. Sugiyama, E. Ito, K. Seki, *Adv. Mater.* **1999**, *11*, 605 – 625.
[39] H. Imahori, H. Yamada, Y. Nishimura, I. Yamazaki, Y. Sakata, *J. Phys. Chem. B* **2000**, *104*, 2099 – 2108.
[40] A. J. Bard, L. R. Faulkner, *Electrochemical Methods: Fundamentals and Applications*, Wiley, New York, **2001**.
[41] B. de Boer, A. Hadipour, M. M. Mandoc, T. van Woudenbergh, P. W. M. Blom, *Adv. Mater.* **2005**, *17*, 621 – 625.
[42] Here, the shifted potentials of C_{12} SAMs were approximated by using data of C_{16} alkanethiol reported in ref. [41].
[43] I. Renge, *J. Phys. Chem.* **1995**, *99*, 15955 – 15962.
[44] M. Tanasova, C. Vasileiou, O. O. Olumolade, B. Borhan, *Chirality* **2009**, *21*, 374 – 382.
[45] *Gaussian 09, Revision C.01*, M. J. Frisch, G. W. Trucks, H. B. Schlegel, G. E. Scuseria, M. A. Robb, J. R. Cheeseman, G. Scalmani, V. Barone, B. Mennucci, G. A. Petersson, H. Nakatsuji, M. Caricato, X. Li, H. P. Hratchian, A. F. Izmaylov, J. Bloino, G. Zheng, J. L. Sonnenberg, M. Hada, M. Ehara, K. Toyota, R. Fukuda, J. Hasegawa, M. Ishida, T. Nakajima, Y. Honda, O. Kitao, H. Nakai, T. Vreven, J. A. Montgomery, Jr., J. E. Peralta, F. Ogliaro, M. Bearpark, J. J. Heyd, E. Brothers, K. N. Kudin, V. N. Staroverov, T. Keith, R. Kobayashi, J. Normand, K. Raghavachari, A. Rendell, J. C. Burant, S. S. Iyengar, J. Tomasi, M. Cossi, N. Rega, J. M. Millam, M. Klene, J. E. Knox, J. B. Cross, V. Bakken, C. Adamo, J. Jaramillo, R. Gomperts, R. E. Stratmann, O. Yazyev, A. J. Austin, R. Cammi, C. Pomelli, J. W. Ochterski, R. L. Martin, K. Morokuma, V. G. Zakrzewski, G. A. Voth, P. Salvador, J. J. Dannenberg, S. Dapprich, A. D. Daniels, O. Farkas, J. B. Foresman, J. V. Ortiz, J. Cioslowski, D. J. Fox, Gaussian, Inc. Wallingford, CT, **2011**.

Received: March 25, 2013
Published online on June 21, 2013